An activatable dual polymer nanosystem for photoimmunotherapy and metabolic modulation of deep-seated tumors

Gengqi Liu[a], *Jiexin Li*[a], *Xiaojie Wang*[a], *Ren He*[a], *Yumiao Zhang*[a]*

a School of Chemical Engineering and Technology, Key Laboratory of Systems Bioengineering (Ministry of Education), Frontiers Science Center for Synthetic Biology (Ministry of Education), Tianjin University, P. R. China, 300350

*E-mail: ymzhang88@tju.edu.cn.

Key words: Photothermal therapy, Immunotherapy, NIR-II, Immunometabolic, cancer therapy, Semiconducting polymer, nano micelle.

Abstract: Nanomedicine in combination with immunotherapy has shown great potential in the cancer treatment, but phototherapeutic nanomaterials that specifically activate the immunopharmacological effects in deep tumors have rarely been developed due to limited laser penetration depth and tumor immune microenvironment. Herein we report a newly

This article has been accepted for publication and undergone full peer review but has not been through the copyediting, typesetting, pagination and proofreading process, which may lead to differences between this version and the Version of Record. Please cite this article as doi: 10.1002/adhm.202303305.

synthesized **s**emiconducting **p**olymer grafted with imiquimod **R**837 and **in**doxmid encapsulated **m**icelle (SPRIN-micelle) with strong absorption in the second near infrared window (NIR-II) that can relieve tumor immunosuppression and enhance the photothermal immunotherapy and catabolic modulation on tumors. Immune agonists (Imiquimod R837) and immunometabolic modulators (Indoxmid) were covalently attached to NIR-II semiconducting polymer (SP) sensors via a glutathione (GSH)-responsive self-immolation linker and then loaded into Pluronic F127 (F127) micelles by a temperature-sensitive critical micelle concentration (CMC)-switching method. Using this method, photothermal effect of SPRIN-micelles in deep-seated tumors could be activated, leading to effective tumor ablation and immunogenic cell death. Meanwhile, imiquimod and indoxmid were tracelessly released in response to the tumor microenvironment, resulting in DC maturation by imiquimod R837 and inhibition of both indoleamine 2,3-dioxygenase (IDO) activity and Treg cell expression by indoxmid. Ultimately, cytotoxic T lymphocyte infiltration and tumor metastasis inhibition in deep solid tumors (9 mm) were achieved. In summary, this work demonstrates a new strategy for the combination of photothermal immunotherapy and metabolic modulation by developing a dual functional polymer system including activable SP and temperature-sensitive F127 for the treatment of deep solid tumors.

Introduction

Immunotherapy has revolutionized cancer treatment by harnessing the host immune system for innate and acquired immunity against tumors[1, 2]. However, the clinical success of

cancer immunotherapy is hindered by tumor immunosuppressive microenvironment (TiME) featuring inferior T cell infiltration, inactivation of the interferon pathway, and defective antigen presentation[3, 4]. Therefore, other therapeutic modalities are complementarily used with cancer immunotherapy to enhance the treatment efficacy[5], such as chemotherapy[6, 7], phototherapy[8, 9], radiotherapy[10, 11] and corresponding nanomedicines with improved therapeutic efficacy and reduced side effect hold great potential for seamless integration of these treatment paradigms.

Photothermal therapy (PTT) using phototransducers for the generation of heat has evolved as an important therapeutic approach for cancer ablation[12, 13]. PTT can also lead to immunogenic cell death (ICD) that enables activation of immune responses[14, 15]. However, the treatment of orthotopic and deep-seated tumors by phototherapy is challenging due to the limitation of laser penetration depth. As such, laser with maximum wavelength in the second near infrared window (NIR-II, 1000–1300 nm) that possesses better biological transparency, lower maximum allowable exposure limits and deeper penetration depth has been focused. Inorganic NIR-II photothermal agents include copper sulfide[16, 17], gold nanoparticle[18, 19], quantum dot[20, 21] and carbon nanotubes[22, 23]. Organic materials with strong absorption in the NIR-II window such as porphyrins[24, 25], phthalocyanines[26, 27], cyanine dyes[28, 29] and semiconducting polymers (SPs) have also emerged with better biocompatibility. Among them, SPs with donor-acceptor (D-A) structure has the advantages of good photostability and high extinction coefficient, holding potential for use of

photoimmunotherapy[30-32]. For instance, semiconductor polymer and toll-like adjuvant (R848) encapsulated thermo-responsive liposome has been developed that could release R848 and induce ICD on demand in tumors upon NIR-II light irradiation, ultimately giving rise to the inhibition of tumor growth and metastasis[33]. Another approach to increase penetration depth is rational design of ultraconcentrated photothermal agents. We have reported a series of micellar photothermal agent of high concentration (absorption over 100-1000) made by a surfactant-stripping method that can achieve a tissue penetration depth over 13 cm, allowing for deep tissue photothermal therapy[34-36] and photoacoustic (PA) imaging[37-40].

Moreover, to overcome off-target and toxicity issues[41-43], stimulus-responsive nanoparticles that specifically release antigens and adjuvants in a controllable fashion have been explored in responsive to various stimuli such as pH[44, 45], temperature[46, 47], redox conditions[48, 49], and enzymes[50, 51]. For instance, Liang et al. designed a pH-sensitive nanovaccine for the formation of nanosheets that can disrupt endosomes to allow antigenic peptides to effectively undergo endosomal escape and activate the immune system[52]. In addition, given the high redox environment and abundant enzymes in tumor microenvironment, endeavors have been focused on design of redox-responsive or enzyme-responsive subunit vaccines to improve the tumor targeting and significantly enhance the immunotherapeutic effect but with less systemic toxicity[53, 54].

To boost immune responses, immunoadjuvants including toll-like receptor (TLR)-agonists[55], inorganic adjuvants such as alum[56], plant derivatives such as saponin[57],

bacterial membrane[58], endogenous proteins[59] and synthesized compounds[60] have been used for cancer immunotherapy. However, studies for the alleviation of TiME by immunometabolic modulators have been relatively rarely reported. Immune cells activated by immune adjuvants release interferon and other cytokines which also stimulate the expression of genes encoding enzymes promoting tryptophan (Trp) and arginine (Arg) catabolism, including indoleamine 2,3 dioxygenase (IDO), arginase 1 (ARG1) and inducible nitric oxide synthetase (iNOS)[61]. Persistent Trp catabolism suppresses the immune response at the tumor sites and impairs the immunotherapeutic effect[62]. Therefore, one strategy to achieve synergistic immunotherapeutic effects is the combination of activation immune responses by adjuvants and regulation of immune metabolism to reprogram the TiME. Some clinically used immune metabolism modulators for TiME regulation include Indoximod (IND), Navoximod (NLG919), Epacadostat (INCB024360)[63, 64]

Taking the afore-mentioned points together, we herein report a GSH-responsive nanotherapeutic micelle (SPRIN-micelle) for photothermal immunotherapy of deep-seated tumors using a laser in the NIR-II window (**Figure 1**). SPRIN-micelle consists of a NIR-II semiconducting polymer (SP) backbone as a phototransducer in conjugation with the potent TLR7 agonist (imiquimod, R837) as an immune agonist and an indoleamine 2,3-dioxygenase (IDO) inhibitor (indoximod, IND) via a GSH-responsive self-immolative linker (SL) (**Figure 1A**). R837 mainly acts on antigen-presenting cells (APCs) such as dendritic cells (DCs) to stimulate the secretion of key pro-inflammatory cytokines and to promote DC maturation,

ultimately resulting in T-lymphocyte differentiation and proliferation[65]. IND alleviates IDO-induced Trp catabolism within cancer cells and DCs, and then relieving immunosuppression caused by the Trp metabolite Kyn[66]. Under NIR-II light radiation, the photothermal effect and ICD induced by SPRIN-micelle directly ablate tumors and promote antitumor immunity. R837 and IND are responsively released in the presence of high levels of intracellular GSH in tumors, that induce immune activation and relieve immunosuppression (**Figure 1B**). Using temperature-sensitive Pluronic micelles, concentrated SPRIN-micelle with strong absorption in the NIR-II window enables laser penetration in deep tissues and photothermal immunotherapy. Ultimately, primary tumors are completely eradicated in deep tissues and distant tumors are also effectively suppressed without causing significant systemic toxicity.

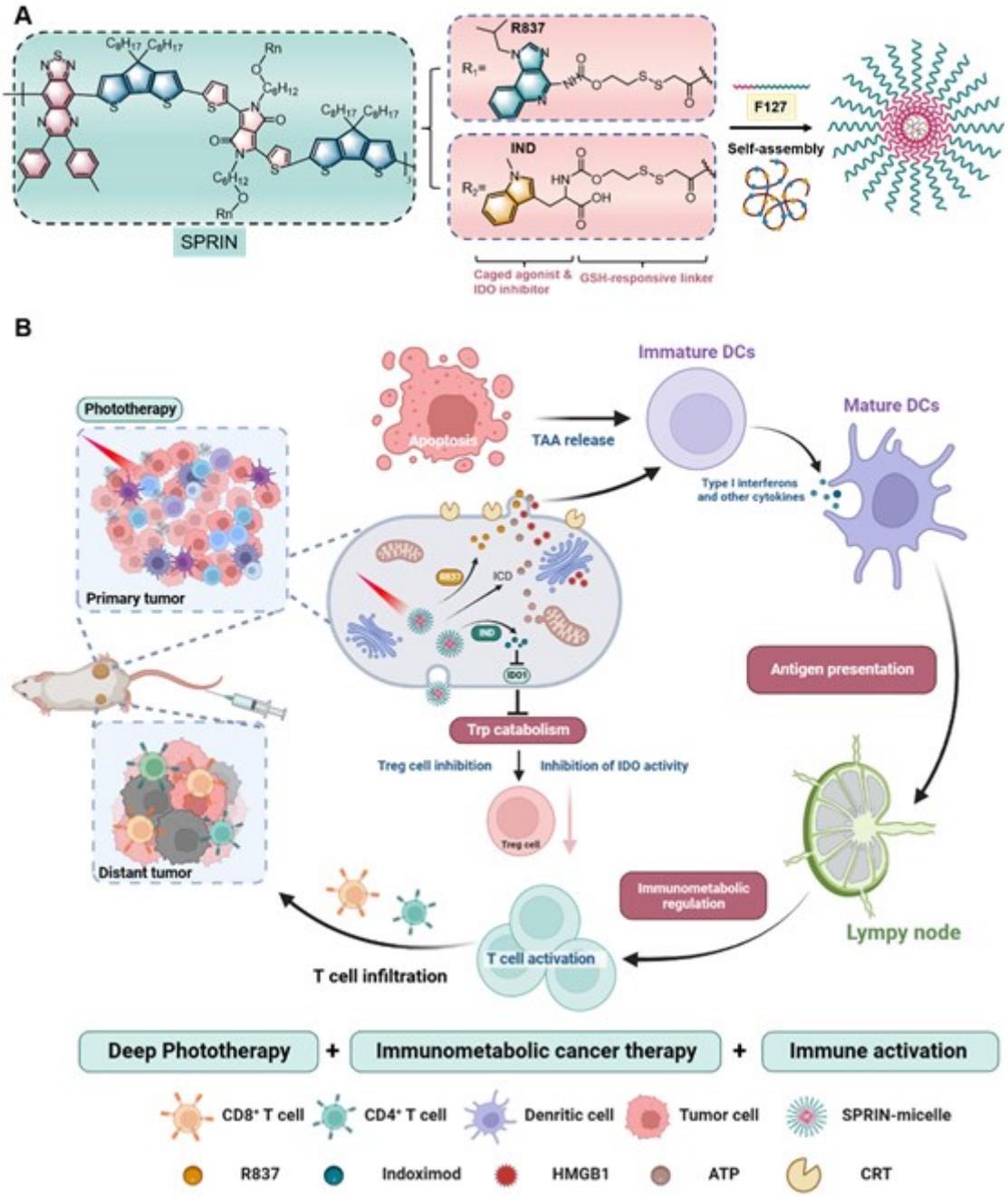

Figure 1. Schematic illustration of SPRIN-micelle-mediated for co-therapy of cancer photoimmunotherapy. A) Structure of SPRIN and SPRIN-micelle. B) SPRIN-micelle-mediated activatable photo-immune co-therapy consists of two processes: (i) deep photothermal therapy triggers a series of cancer immune responses, including immunogenic cell death (ICD), tumor-associated antigen release, and promotion of DC maturation; (ii) the specific release of immune adjuvants (R837) and immunometabolic modulators(IND) from SPRIN-micelle in the presence of high intracellular GSH levels that promotes DC maturation, inhibits IDO-induced Trp hypermetabolism, subsequently resulting in immunosuppression alleviation and immune responses activation.

Result and discussion

Synthesis and in vitro characterization

Hereinafter, SPR, SPIN and SPRIN mean SP conjugated with R837, IND, and both, respectively. And their F127 micellar forms was denoted as SPR-micelles, SPIN-micelles and SPRIN-micelles, respectively. To synthesize the NIR-II-absorbing semiconductor polymer precursor SPRIN, three backbone monomers were copolymerized by Stille polycondensation including 4,4-dioctyl-2,6-bis-(trimethylstannyl)-4H-cyclopenta[2,1-b:3,4-b]dithiophene(CDT), 4,9-Dibromo-6,7-bis(4-methylphenyl)[1,2,5]thiadiazolo[3,4-g]quinoxaline (DDTQ) and 2,5-bis(6-bromohexyl)-3,6-bis(5-bromo thiophen-2-

yl)pyrrolo[3,4-c]pyrrole-1,4(2H,5H)-dione (DPP-Br) (**Figure 2A and Figure S1C**). In order to conjugate amine-containing R837 (as an immune agonist) and IND (as an immunometabolic modulator) to SP, an amine-reactive and glutathione (GSH)-labile self immolative linker (SL) was first connected to amines on R837 or IND, followed by reaction with thioglycolic acid. Next, the carboxyl groups were activated with oxalyl chloride by chlorination to obtain SL-R837 / IND-Cl so that R837 and IND could be tracelessly released in tumor microenvironment overexpressing GSH (**Figure S1A**). SP-TBSO was converted to SP-OH after deprotection by TBAF to restore the hydroxyl group on the branched chain. Finally, SP-IR was obtained by esterification reaction between SP-OH and SL-R837 or SL-IND (**Figure S1B, C**). To improve the solubility, SP-IR were encapsulated in Pluronic F127 (F127) micelles, followed by stripping away excess F127 by ultrafiltration at low temperature, generating concentrated and purified SPRIN-micelles that enable laser penetration in deep seated tumors[34, 38-40]. Gel permeation chromatography (GPC) analysis demonstrated that the average molecular weight (MW) of SP-OH was 5052 (**Figure S2**). All the intermediates were characterized by ^{1}H/ ^{13}C NMR and ESI-MS as shown in **Figure S3–24**.

Optical and colloidal properties of SP as well as SPRIN-micelles were also investigated. Dynamic light scattering (DLS) and transmission electron microscopic (TEM) image showed that the size of SPRIN-micelles (68 nm) is slightly larger than that of SP-micelles (58 nm)

(**Figure 2B**), presumably owing to the presence of hydrophobic linkers. Negligible size variation was observed for both SP-micelles and SPRIN-micelles during storage in PBS solution and FBS solution (10%) for 3 days (**Figure S25**), indicating their favorable colloidal stability. SP and SPRIN-micelle have similar absorption spectra with a maximum at 940 nm in the NIR-II window (**Figure 2C**), suggesting that conjugation of R837 and IND to the SP backbone did not affect its optical properties. In addition, the molar extinction coefficient of SRPIN-micelles in F127 aqueous solution was calculated to be 4.82 mL (mg.cm) $^{-1}$, which is almost the same as that in organic solvent such as tetrahydrofuran (THF) (**Figure S26**).

As demonstrated in Figure 2D, upon the 940 nm laser irradiation for 10 min, similar to SP, the temperature of SPRIN-micelles (50μg mL^{-1}) increased up to 56°C. In contrast, the temperature of the PBS solution was almost unchanged under the same irradiation conditions (**Figure S27**). In addition, the photothermal stability of SPRIN-micelles (100 μg mL^{-1}) was evaluated under continuous NIR-II (940 nm) photoirradiation. Five temperature change cycles of SPRIN-micelle solution were obtained by controlling laser on and off. Induced a significant temperature rise in the aqueous solution (**Figure 2E**). After irradiation for 10 min, the maximum temperature of SPRIN-micelle solution was 68°C and negligible changes in the maximum temperature of SPRIN-micelle were observed during the five heating and cooling cycles, indicating its good photostability. In addition, SPRIN-micelles has a high

photothermal conversion efficiency of about 49.2% at 940 nm (**Figure S28**) and about 53% at 1064 nm, respectively (**Figure S29**).

The GSH-responsive traceless release properties of SPRIN-micelles were evaluated and analyzed by high performance liquid chromatography (HPLC) (**Figure 2F, G, Figure S30**). The release of free R837 and IND by SPRIN-micelles as well as SPR-micelles (or SPIN-micelles) could not be detected in the absence of GSH, whereas in a PBS solution containing 10 mM GSH, release of R837 and IND was observed and reached a plateau close to 100% at about 4 h.

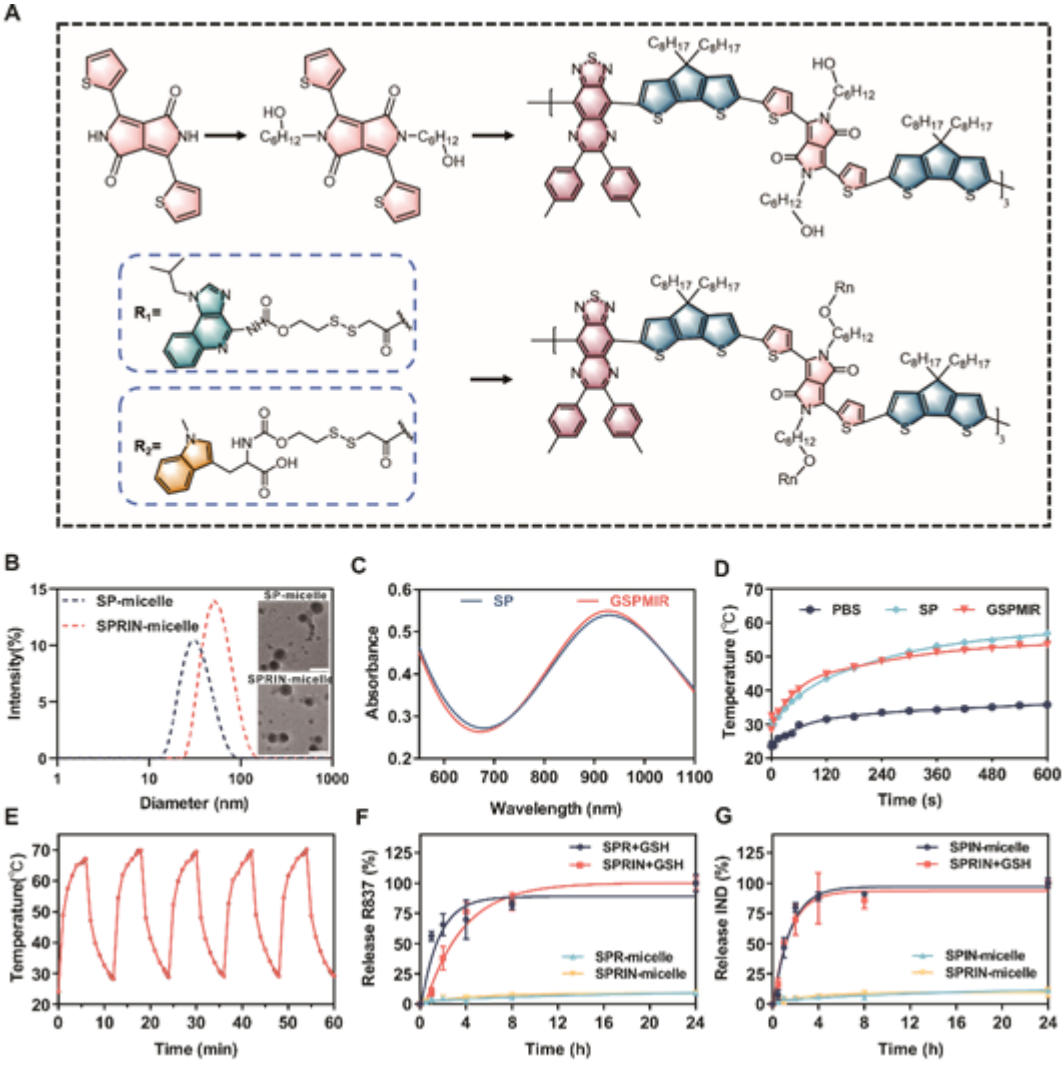

Figure 2. Preparation and characterization of SPRIN-micelles. A) Synthesis route of SPRIN-micelles, see supporting information for more details. I) 3,6-dithiophen-2-yl-2,5-dihydropyrrolo [3,4-c]pyrrole-1,4-dione, 1-bromo-6-hexanol (DPP), N,N-dimethylformamide (DMF), 120°C, 12 h. ii) Tert-butyldimethylsilyl chloride, Dichloromethane (DCM), 25°C, 12 h; N-Bromosuccinimide, Trichloromethane, 0 °C, 12 h iii) 4,4-dioctyl-2,6-bis-(trimethylstannyl)-4H-cyclopenta[2,1-b:3,4-b′]dithiophene (CDT), 4,9-Dibromo-6,7-bis(4-methylphenyl)[1,2,5]thiadiazolo[3,4-g]quinoxaline (DDTQ), tris-(o-tolyl)phosphine , Tris

(dibenzylideneacetone) dipalladium ($Pd_2(dba_3)$), Chlorobenzene, 110 °C, 24 h; Tetrabutylammonium fluoride (TBAF), tetrahydrofuran(THF), 25°C, 12 h; Cl-SL-R837, Cl-SL-IND, DCM, N,N-Diisopropylethylamine (DIPEA). B) Size distribution using DLS measurement and TEM image of SP-micelles and SPRIN-micelles (scale bar = 100 nm). C) Absorption spectra of SP-micelles and SPRIN-micelles in PBS buffer. D) Photothermal effect of PBS, SP-micelles and SPRIN-micelles under 940 nm laser irradiation at 1 W cm^{-2}. Concentration of SP and SPRIN are both 50 μg mL^{-1}. E) Photostability of SPRIN-micelles ([SP or SPRIN] = 100 μg mL^{-1}) investigated by five photothermal heating (940 nm photoirradiation, 1 W cm^{-2}, 6 min) and cooling (natural cooling with laser off for 6 min) cycles. Release kinetics of F) R837 and G) IND from SPRIN-micelles, SPIN-micelles or SPR-micelles with or without GSH (10 mM) in PBS buffer.

Photothermal immunotherapy and catabolic modulation

Next, the photothermal effect of SPRIN-micelles was investigated using CT26 tumor cells. Without shedding laser, the cytotoxicity of SPRIN-micelles on CT26 cells was negligible whereas SPRIN-micelles with 940 nm laser induced significant cell death (**Figure 3A**). For instance, the cell viability after treatment of 50 and 100 μg mL^{-1} SPRIN-micelles with 940 nm laser decreased to 48% and 25%, respectively. We next evaluated the cellular uptake of SPRIN-micelles by CT26 cancer cells. SPRIN-micelle was fluorescently labelled by

fluorescein 5-isothiocyanate (FITC) using amine-modified F127 instead of hydroxyl-terminated F127 for micelle preparation. Cellular uptake of SPRIN-micelles reached saturation at about 4 h (**Figure S31**). As shown in Figure 3B, evident green fluorescence was observed in cytoplasm after CT26 cells were treated by fluorescently labelled SPRIN-micelles, indicating efficacious endocytosis of SPRIN-micelle in CT26 cells. Notably, the cell death of should be ascribed to both photothermal and photodynamic effect although the focus of this work was put on the former. As shown in Figure S32, SPRIN-micelle could also generate singlet oxygen via a photodynamic effect upon exposure to laser irradiation, indicated by using 2`,7`-dichlorodihydrofluorescein (DCFH) as a ROS probe.

To evaluate the immunogenic cell death (ICD) by SPRIN-micelles, exposure or release of important damage associated molecular patterns (DAMPs) in dying tumor cells upon laser irradiation were examined including calreticulin (CRT), high mobility group box 1 (HMGB1), and adenosine triphosphate (ATP). After treatment by SPRIN-micelles for 24 hours, CT26 cancer cells were incubated for additional 4 hours after 940 nm photoirradiation for 10 minutes. A significant upregulation of CRT was found in CT26 cells after treatment with SP-micelles and SPRIN-micelles under 940 nm photoirradiation, which was evidenced by fluorescence microscopic images of CRT on the cell surface after treatment by SP-micelles or SRPIN-micelles, which was also confirmed by elevated MFI of APC-labeled anti-CRT antibodies (10.1-fold) (**Figure 3C,S33**). Meanwhile, the difference in CRT exposure with and without photoirradiation was also analyzed by flow cytometry and a 3.4 to 3.6-fold

increase in fluorescence was observed (**Figure S34**). The release of HMGB1 from the SP-micelles, SPIN-micelles, SPR-micelles or SPRIN-micelles groups with laser irradiation groups was 1.9- to 2.6-fold higher than without photoirradiation (**Figure 3E**). Similarly, the release of ATP induced by laser was 6- to 9.2-fold higher than that in control groups without laser irradiation.

The potential of use of SPRIN-micelles for immunotherapy against cancer cells was assessed using bone marrow-derived dendritic cells (BMDCs). Dendritic cells are crucial in antigen presentation, linking innate and adaptive immunity. Enhanced DC maturation initiates T cell activation and generations of $CD8^+$ T cells killing tumor cells[67, 68]. However, IDO expressed in tumor cells promotes tryptophan hypermetabolism, which in turn yields an immunosuppressive effect[62, 69]. To verify the reversal effect immunosuppression microenvironment by SPRIN-micelles, we pretreated CT26 cells with SPRIN-micelles for 12 h, followed by photoirradiation with 940 nm laser for 10 minutes. After incubation for additional 24 h, DCs were added and co-cultured with CT26 cells for 48 h. DC maturation was characterized by quantifying the expression of CD40 and CD86 by flow cytometry. The expression of mature DC receptors ($CD40^+$, $CD80^+$, $CD86^+$) is significantly higher in the light-irradiated group than the groups with no laser treated (**Figure 3G, Figure S35, S36, S37**). Then to verify the capability of SPRIN-micelles to directly induce DC maturation, we co-incubated SPRIN-micelles with DCs for 24 h. The expression of receptors $CD40^+$ $CD80^+$and $CD86^+$ was also examined using flow cytometry. We identified significantly

higher expression of mature dendritic cell receptors ($CD40^+$, $CD86^+$ and $CD80^+$, $CD86^+$) in the SPRIN-micelles group (75.3% and 51.9%) than in the other control groups including SP-micelles, SPR-micelles and SPIN-micelles (**Figure S38, S39**). It may be that DCs also express IDO to promote tryptophan hypermetabolism and cause immunosuppression[70]. In addition, the cytokine levels in the cell supernatant in the experiments above were also investigated. SPRIN-micelles, SPIN-micelles, and SPR-micelles significantly promoted the secretion of cytokines from DCs after treatment, and SPRIN-micelles induced more secretion of IFN-γ and TNF-α from DCs than SPIN-micelles and SPR-micelles (**Figure S40**). This demonstrates that R837 and IND can synergistically boost immune response. Also, the cytokine levels in the cell supernatant in the light- irradiated groups were significantly higher than those without laser irradiation (**Figure S41**), which further demonstrates the immune effect induced by ICD.

Indoleamine-2,3-dioxygenase 1 (IDO-1) was shown to suppress T cell responses by activation of regulatory T (Treg) cells. Transition of tryptophan (Trp) into kynurenine (Kyn) as downstream of IDO-1 involves in suppression of immune cells via the formation of immunosuppressive catabolites. Here, IND was used as an immunomodulator to inhibit the Trp metabolism, ultimately resulting in inhibition of Treg and promotion of immune response. Therefore, we next evaluated the immunomodulation IND-grafted SPRIN-micelles by first pre-treatment of CT26 cells with IFN-γ (100 ng mL^{-1}) to induce intracellular IDO overexpression, followed by incubation with SPRIN-micelles and then measurement of the

downstream product Kyn in the cell culture medium by high performance liquid chromatography (HPLC). As shown in Figure 3H, SPRIN-micelles and SPIN-micelles induced a 2-fold reduction of Kyn content in the cell culture medium in comparison to that of control groups. This suggests that IND released by SPRIN-micelles and SPIN-micelles effectively inhibited IDO activity in CT26 cells, which in turn inhibits Kyn production. Western blotting assay was then performed to further verify the expression of IDO-1. Similarly, CT26 cells were first pretreated with IFN-γ to induce intracellular IDO overexpression, and then SPRIN-micelles was co-incubated with CT26 cells for 24 h. After 940 nm laser irradiation, CT26 cells were collected for total protein extraction. As shown in **Figure 3I**, after irradiation, IDO1 expression was significantly downregulated by both SPRIN-micelles and SPIN-micelles.

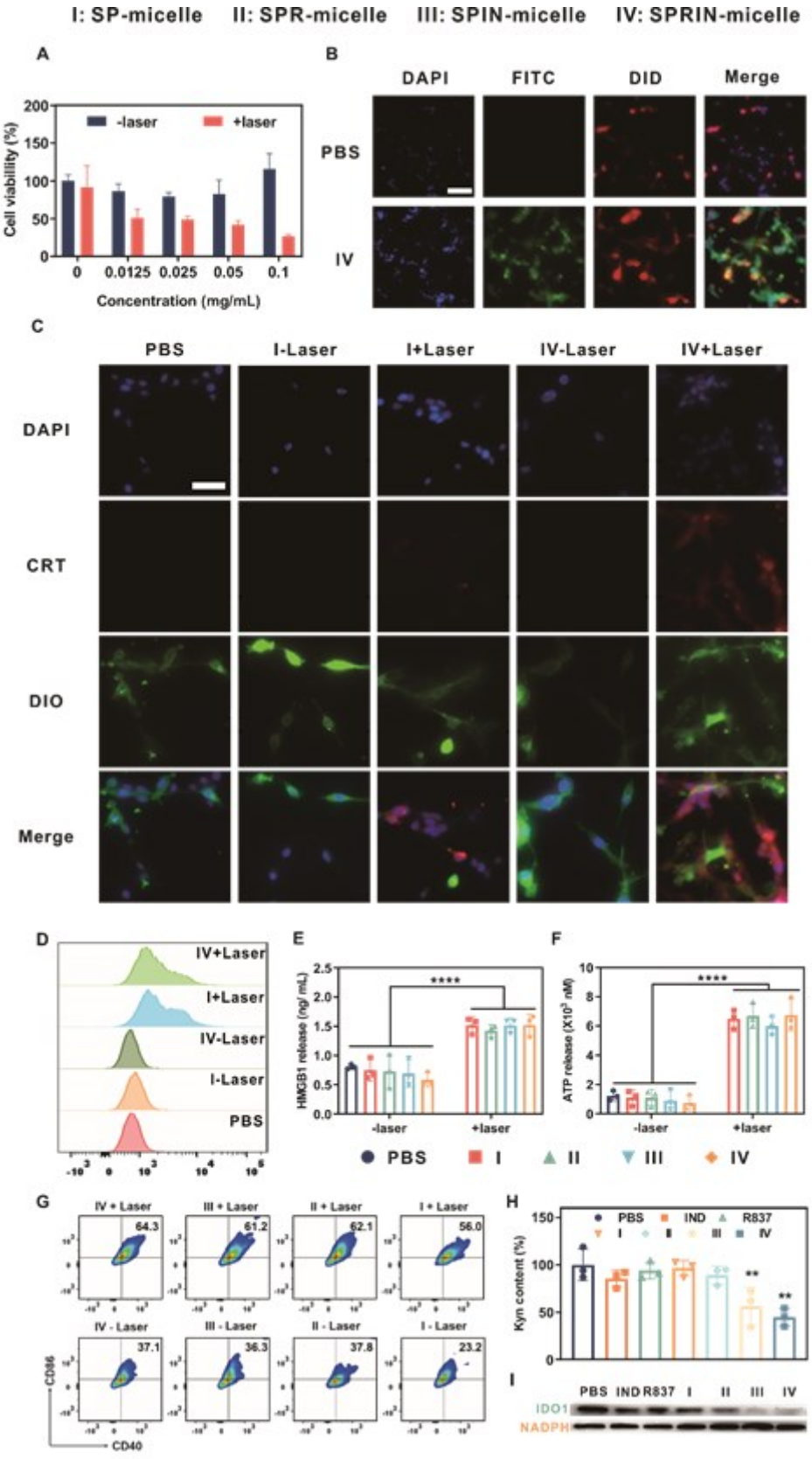

Figure 3. Photothermal immunotherapy and catabolic modulation by SPRIN-micelles A) Viability of CT26 cells at 12 h after treatment with SPRIN-micelles at different concentrations with or without 940 nm photoirradiation. (1 W cm^{-2}, 6 min) (n = 3). B) Fluorescence images of cellular internalization (24 h) of SPRIN-micelles ([SP] = 50 μg mL−1) in CT26 cancer cells. SPRIN-micelles were labeled with fluorescein 5-isothiocyanate (FITC) (Scale bar=200 μm). Blue, green and red fluorescence indicate nuclei staining by 4', 6-diamidine-2'-phenylindole dihydrochloride (DAPI), FITC fluorescently labelled SPRIN-micelles and cell membrane staining by DiD, respectively. C) Fluorescence images of cells after treatment by SPIRN-micelles and staining by AF594-labeled CRT antibody. Blue fluorescence shows the cell nucleus stained with DAPI, red signals show the cell surface expression of CRT from AF594-labeled CRT antibody, and green fluorescence shows the cell membrane stained with DiO (Scale bar=200 μm). D) Representative flow cytometric plots of CRT exposure on cell surface of CT26 cancer cells following treatment by various formulations as indicated (n = 3). HMGB1 extracellular release (E) and ATP extracellular secretion (F) after CT26 cells treated by different formulations as indicated using the HMGB1 ELISA kit and chemiluminescence ATP determination kit, respectively (n = 3). G) BMDCs were treated by different SP formulations for 24 h, followed by analysis of CD40 and CD86 expression by flow cytometry. H) Relative Kyn content in the cell culture medium after CT26 cells were treated by different formulations for 12 h, quantified by HPLC (n=3) ([SP]=50 μg mL^{-1}). I) IDO1 protein expression in CT26 cells evaluated by western blotting

assay ([SP]=50 μg mL^{-1}) after treatment by different formulations as indicated. Statistical significance was calculated via one-way ANOVA with Tukey's test: *p < 0.05; **p < 0.01; ***p < 0.001; ****p < 0.0001.

SPRIN-micelles enable photothermal activation and immunogenicity of deep-seated tumors using laser in the second near infrared (NIR) windows

Next, we investigated SPRIN-micelle-mediated photothermal immunotherapy at different tumor tissue depths upon laser irradiation of different wavelengths (**Figure 4A**). Although the immunogenicity of PTT has been studied and applied in many studies, the photothermal immunotherapy effect at different tissue penetration depths in tumors has not been seldomly investigated. Given that SPRIN-micelles have similar optical absorption at near 860 nm and 1064 nm (**Figure 4B**), we chosen two different light sources of 860 nm or 1064 nm for the next comparative study. In addition, owing to the temperature-sensitivity of F127, CMC switching technology was enabled to strip away excess free surfactant by ultrafiltration at low temperature, generating concentrated SPRIN-micelles with calculated absorbance up to 60, which is about over 60-folds higher than that made by regular preparation methods. (**Figure 4C**). Thus, concentrated SPRIN-micelles with high absorption intensity could be more favorable for photothermal immunotherapy of deep tissues. The SPRIN-micelle aqueous solution was irradiated in vitro by 860 nm and 1064 nm and the temperature of samples shed with 1064 laser was significantly higher than that with 860 nm laser (**Figure 4D**). Next the

temperature increase comparison was conducted again in vivo on tumor-bearing mice treated SPRIN-micelles and 860 nm or 1064 nm laser irradiation for 10 min. The tumor surface temperature (**Figure 4E**) and the intratumoral temperature at different tissue depths (**Figure 4F and 4G**) were monitored. The maximum tumor surface temperature in the 1064 nm group was consistently higher than that in the 860 nm group. Also, the intratumoral temperature gradually decreased as the tissue depth increased, but the temperature in the 1064 nm group was significantly higher than that in the 860 nm group, and could still reach 40°C in the tumor at depth of 9 mm (**Figure 4F, G**), demonstrating the stronger tissue penetration ability of NIR-II light with higher wavelength. To further assess the photothermal immunotherapy at different penetration depths, the tumors were harvested and sectioned from tumor-bearing mice after various treatments as indicated. Firstly, Hematoxylin and eosin (H&E) staining was conducted on tumor sections, and we found that tumor tissues in the 1064 nm group showed significant tissue dissociation and cell apoptosis at 9 mm, whereas the PBS and 860 nm groups showed no significant changes at the same depth (**Figure S42**). In addition, the expression levels of representative biomarkers of apoptosis (Cas-3), ICD (HMGB1) and DC maturation (CD86) were evaluated by immunofluorescent staining of tumor sections (**Figure 4H**). The expression levels of all three biomarkers were downregulated with increasing photothermal depth in both groups treated by the 860 nm and 1064 nm lasers (**Figure S43**). Particularly, in deep tumor tissues (6 mm or 8 mm), the 1064 nm group exhibited a more pronounced biomarker upregulation compared to the 860 nm group, which demonstrates that

NIR-II photothermal therapy can induce enhanced ICD and immune activation in deep tumor tissues, which is more difficult to be realized by NIR-I light.

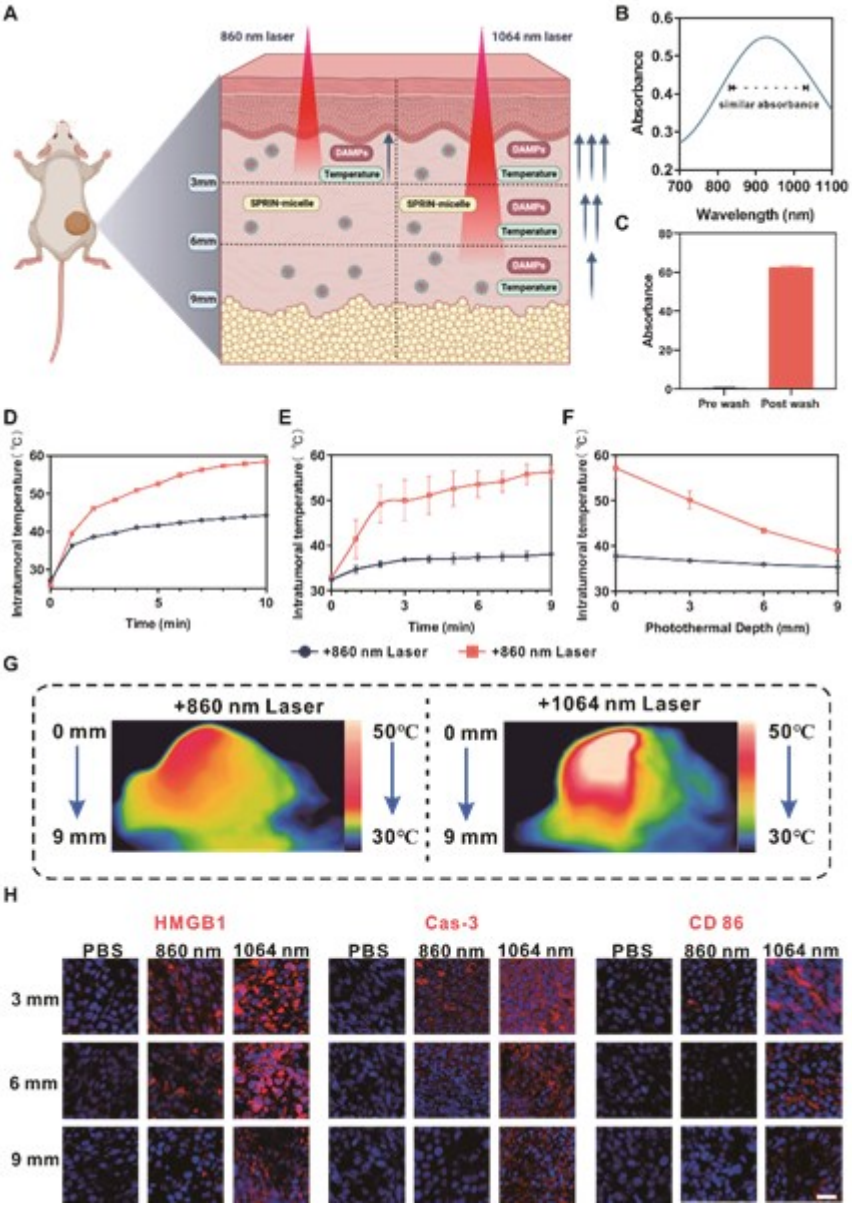

Figure 4. Comparative study of photothermal effect and immunogenicity of deep tumors at different penetration depths in tumors induced by 1064 nm laser and 860 nm laser. A) Scheme of photothermal effect after tumors were irradiated with different light sources and comparative study of the immunogenic response at each tumor depth. B) The SPRIN-micelles have similar absorbance around 860 nm and 1064 nm. C) The absorption of SPRIN-micelles before and after stripping away excess surfactant by CMC-switching method. As such, ultraconcentrated SPRIN-micelles were generated, enabling deep tissue penetration by laser. (n = 3). D) Temperature change of SPRIN-micelle aqueous solutions (SP= 2 mg mL^{-1}) under irradiation by different light sources. E) Maximum temperature on tumor surface of CT26 tumor bearing mice during photoirradiation (n = 3). F) Temperature change and G) thermal image of the tumor at different depths under irradiation of different lasers (n = 3). H) Immunofluorescent images of HMGB1, Cas-3 and CD86 in tumor sections at different depths after SPRIN-micelles-mediated photothermal immunotherapy with different laser treatments. Cas-3, HMGB1 and CD86 are all indicated by red colors. Blue fluorescence indicated nuclei staining by DAPI (Scale bar: 20 μm).

In vivo photothermal immunotherapy.

SPRIN-micelle-mediated photoimmunotherapy was further investigated in vivo using CT26 tumor-bearing BALB/c mice. CT26 cells were inoculated subcutaneously on the right side of the mice as primary tumors; 10 days later, CT26 cells were inoculated subcutaneously on the left side of the mice as distant tumors (**Figure 5A**). After 3 days, CT26 tumor-bearing

mice were intravenously administered 20 mg/kg SP-micelles, SPRIN-micelles, SPIN-micelles and SPR-micelles, subsequently the primary tumor was irradiated by a NIR-II laser (940 nm). The tumor surface temperature in the SP-micelle, SPRIN-micelle, SPIN-micelle and SPR-micelle groups consistently increased to 60°C (**Figure S44**). Afterwards, the growth of primary and distant tumors was monitored for 14 days. Photothermal immunotherapy was assessed by irradiating the primary tumor with NIR light after 24 hours of nanoparticle injection. After treatment, the growth of primary tumors in the SP-micelle, SPRIN-micelle, SPIN-micelle and SPR-micelle groups were all delayed compared to the PBS control group. In particular, the primary tumors in the SPRIN-micelle-treated group were completely inhibited without no noticeable growth. The distant tumors were also completely irradiated only in the SPRIN-micelle-treated group and for other groups the growth of tumors was only delayed, but not inhibited (F**igure 5B, C, F, G, S45**). In addition, the survival curve and individual tumor growth of each mouse were shown in **Figure 5D, F-G**. To verify the suppression of tumor cell growth by the immune effect induced by the SPRIN-micelles, survived mice in the treatment group were rechallenged by injection of CT26 cells on day 60 and no tumor regrowth was observed for another 30 days (**Figure 5E, S51**).

To assess the biocompatibility of SPRIN-micelles, body weight and histological analysis of major organs of mice treated by PBS or SPRIN-micelles were recorded and investigated. No significant difference in body weight was observed in mice injected with PBS, SP-micelles, SPRIN-micelles, SPIN-micelles and SPR-micelles during 14 days (**Figure S46**). Afterwards,

H&E-stained images of the major organs (heart, liver, spleen, lungs and kidneys) of mice injected with SP-micelles, SPRIN-micelles, SPIN-micelles and SPR-micelles showed similar physiological morphology compared to mice injected with PBS (**Figure 5H, Figure S47**). In addition, we performed tissue sections and H&E staining of primary and distant tumors in controls including PBS, SP, SPR-micelle, and SPIN-micelle groups and found no significant tissue dissociation or cell death (**Figure S48**). Furthermore, the biodistribution analysis showed that SPRIN-micelle exhibited the highest accumulation in the liver among major organs (**Figure S49**). As shown in **Figure S50**, the serum chemistry profiles of mice treated with SPRIN-micelles or PBS showed no difference, indicating that intravenous injection of SPRIN-micelles and laser irradiation induced no overt acute toxicity in *vivo*.

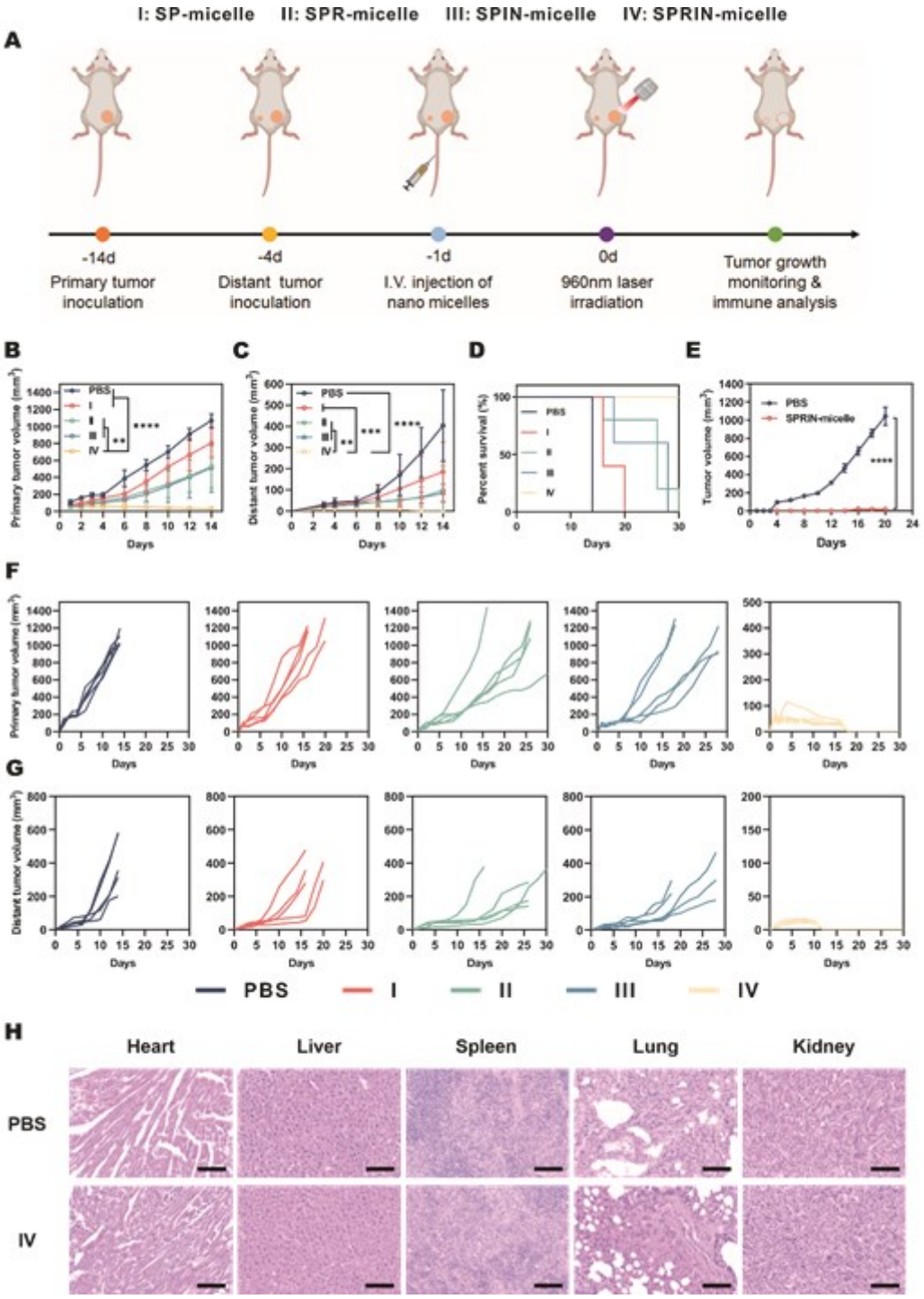

Figure 5. In vivo photothermal immunotherapy by SPRIN-micelles with NIR-II laser. A) Schematic illustration of in vivo anti-cancer therapy. B–C) Tumor growth curves of B) primary and C) distant tumor in living mice after various treatments as indicated (14 days, n = 5). D) Survival curves of CT26-tumor-bearing mice after various treatments as indicated (n = 5). E) Tumor growth curves of CT-26 tumor in surviving mice (n=3). F) Primary tumor and G) distant growth was monitored every other day after treatments as indicated (30 days n=5). H) Hematoxylin and eosin analysis of major organs after systemic injections of different formulations as indicated, Scale bars = 50 μm. Statistical significance of tumor growth and survival rate was analyzed via two-way ANOVA with Tukey's test and log-rank test, respectively.

Mechanism of activation of immune responses by SPRIN-micelles.

To further investigate the mechanism of immune response by photothermal immunotherapy of SPRIN-micelles, the activation of DCs in the primary and distant TDLNs was assessed by flow cytometry. In agreement with the trend of in *vitro* results (Figure 3G), SPRIN micelle-mediated photothermal immunotherapy elicited the highest levels of DC maturation in both primary (61.3%) and distant tumors (54.8%) (**Figure 6A, B**). Among them, the maturation of DCs in the draining lymph nodes from the primary tumor was 1.4-fold, 1.4-fold, 2.4-fold and 3.1-fold higher than that in SPIN-micelle (44.6%), SPR-micelle (44.4%), SP-micelle (25.7%) and PBS group (19.8%), respectively, while the maturation of DCs in the draining lymph

nodes from the distal tumor was 1.4-fold, 1.6-fold, 2.2-fold and 2.9-fold higher than that in SPIN-micelle (38.4%), SPR-micelle (34.3%), SP-micelle (25.3%) and PBS group (18.6%), respectively. This demonstrates the superior photothermal effect and maturation of DCs induced by SPRIN-micelles and mediated by immune adjuvants (R837) and immunometabolic modulators (IND).

To evaluate the effect of IDO inhibitors and immune adjuvants on photothermal immunotherapy, tumor-infiltrating lymphocytes, including $CD4^+$, $CD8^+$ and Treg cells, were measured by flow cytometry. Among them, the infiltration of $CD4^+$ and $CD8^+$ T cells in primary and distant tumors play a crucial role in killing primary and distant tumors, while Treg cells are responsible for immunosuppression. In the spleen, the SPRIN-micelle group had the highest level of $CD4^+$ (54.2%) and $CD8^+$ (30.2%) T-cell infiltration and the lowest level of Treg cell differentiation (12.5%). In addition, the $CD8^+$/Treg ratio (2.23%) in the SPRIN-micelle group was also significantly lower than that in all other groups, representing 1.78-fold, 2.7-fold, 4.9-fold and 6.4-fold higher than that in the SPIN-micelle (1.25%), SPR-micelle (0.82%), SP-micelle (0.45%) and PBS (0.35%) groups, respectively (**Figure 6C-D**). In contrast, the SPRIN-micelle group had the highest level of $CD8^+$ T cell infiltration and the lowest level of resident Treg in both primary and distant tumors as well. The infiltration rate of CD8+ T cells in the SPRIN-micelle group reached 65.5% and 53.1% in the primary and distal tumors, respectively, which was at least 1.2 times higher than in all other groups (**Figure 6F**, **S52**). In contrast, the rate of Treg cells in primary and distal tumors in the

SPRIN-micelle group was only 17.7% and 18%, which was significantly lower than the rate of Treg cells in all other groups (**Figure 6G**, **S52**). In addition, the ratio of CD8+ cells to Treg cells in primary and distal tumors in the SPRIN-micelle group was 3.6% and 2.92%, respectively, which was at least 1.34 and 1.45 times higher than that in other control groups (**Figure 6H-I**). In addition, we collected blood from mice for the detection of immune cell-derived cytokines such as IL-6, TNF-α, and IFN-γ. We found that SPRIN-micelle mediated photothermal immunotherapy produced the highest levels of immune cell-derived cytokines (IL-6, TNF-α, and IFN-γ) (**Figure 6J-L**). These data suggest that SPRIN-micelle-induced ICD lead to activation of immune responses by generation of cytokines and promotion of $CD8^+$ T cell infiltration with the assistance of R837. Meanwhile, IDO1 inhibitors interference the metabolism of tryptophan, which in turn inhibits the differentiation of Treg cells, demonstrating the immunosuppression reprogramming capability of SRPIN-micelles owing to the presence of IND.

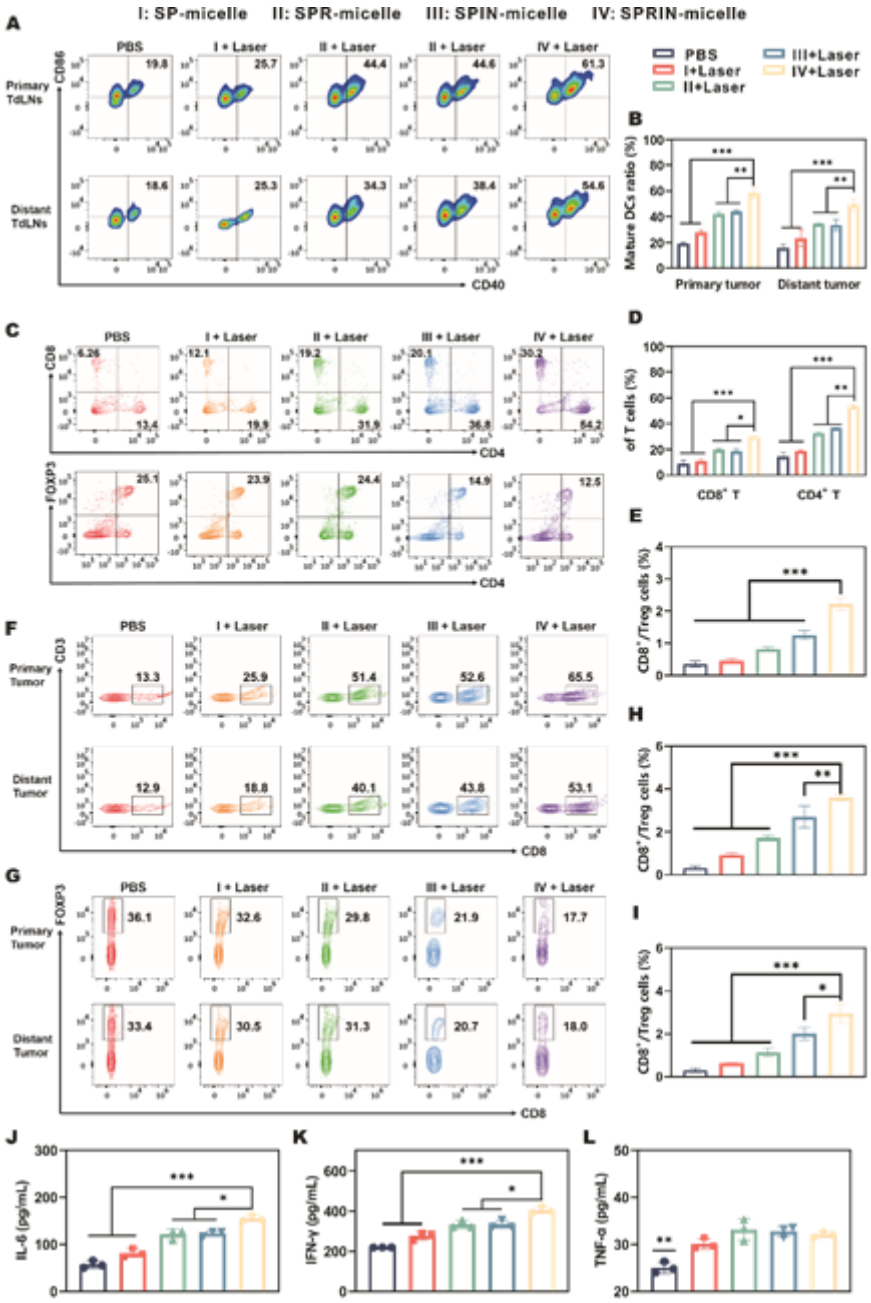

Figure 6. In vivo immune responses after photothermal immunotherapy with SPRIN-micelles. DC maturation measured by flow cytometry after cells in primary A) and B) distant tumor-draining lymph nodes were collected and stained with CD11c, CD40 and CD86 on day 3 (n = 3). C) Representative flow analysis of $CD8^+$ and $CD4^+$ cells and $CD4^+FOXP3^+$ cells

gating on $CD3^+$ cells in the spleen with different treatments on day 7 (n = 3). The value of D) $CD8^+$ and $CD4^+$ and E) $CD8^+$/Treg in spleen after different treatments (n = 3). F) Representative flow cytometry plots and quantitative analysis of F) $CD8^+$ T cells and G) $CD4^+$ T cells (gated on $CD3^+$ T cells) in the primary tumor and distant tumor on day 7 after treatment by different formulations as indicated (n = 3). The value of $CD8^+$/Treg in the H) primary tumor and I) distant tumor after different treatments (n = 3). Cytokine levels of IL-6, IFN-ɣ, TNF-α in serum (pg mL^{-1}) from mice at day 3 after treatment by different formulations as indicated (n = 3). Statistical significance was calculated via one-way ANOVA with Tukey's test: *p < 0.05; **p < 0.01; ***p < 0.001; ****p < 0.0001.

Immune activation in simulated deep-seated tumor model.

In order to investigate the immune activation effect of the SPRIN-micelle on deep-seated tumors, we simulated the deep tumors by superimposing a layer of 1.5 cm chicken breast meat in thickness onto the tumor tissue of mice bearing tumors (**Figure 7A**). Subsequently, lymphocytes were extracted from treated lymph nodes, and T cells from both spleen and tumor tissue were analyzed. The temperature near the tumor tissue reached approximately 42 ℃ when covered with chicken breast (**Figure 7B**). To further investigate the mechanism of immune activation effect of the SPRIN-micelle on deep-seated tumors, the activation of DCs in the TDLNs was assessed by flow cytometry. The expression of mature DC receptors ($CD40^+$, $CD86^+$) is significantly higher in the light-irradiated group than the groups with no

laser treated, representing 3.7-fold higher than that in the no laser treatment group (**Figure 7C, D**).

To evaluate the effect of IDO inhibitors and immune adjuvants on photothermal immunotherapy of deep-seated tumor, tumor-infiltrating lymphocytes, including $CD4^+$, $CD8^+$, were measured by flow cytometry. In spleens, the light-irradiated group had higher level of $CD4^+$ (42.7%) and $CD8^+$ (12.1%) T-cell infiltration than the group with no laser treatment. In contrast, the SPRIN-micelle group had the higher level of $CD4^+$ (37.8%) and $CD8^+$ (23.3%) T cell infiltration than the group with no laser treatment as well. (**Figure 7E, D, F**). Furthermore, we collected serum from the post-treatment mice and subjected to cytokine analysis. We found that the level of cytokine (HMGB1, TNF-α) was significantly higher in the light-irradiated group than the groups with no laser treated, representing 2.84-fold and 1.5-fold higher than that in the no laser group (**Figure S53**).

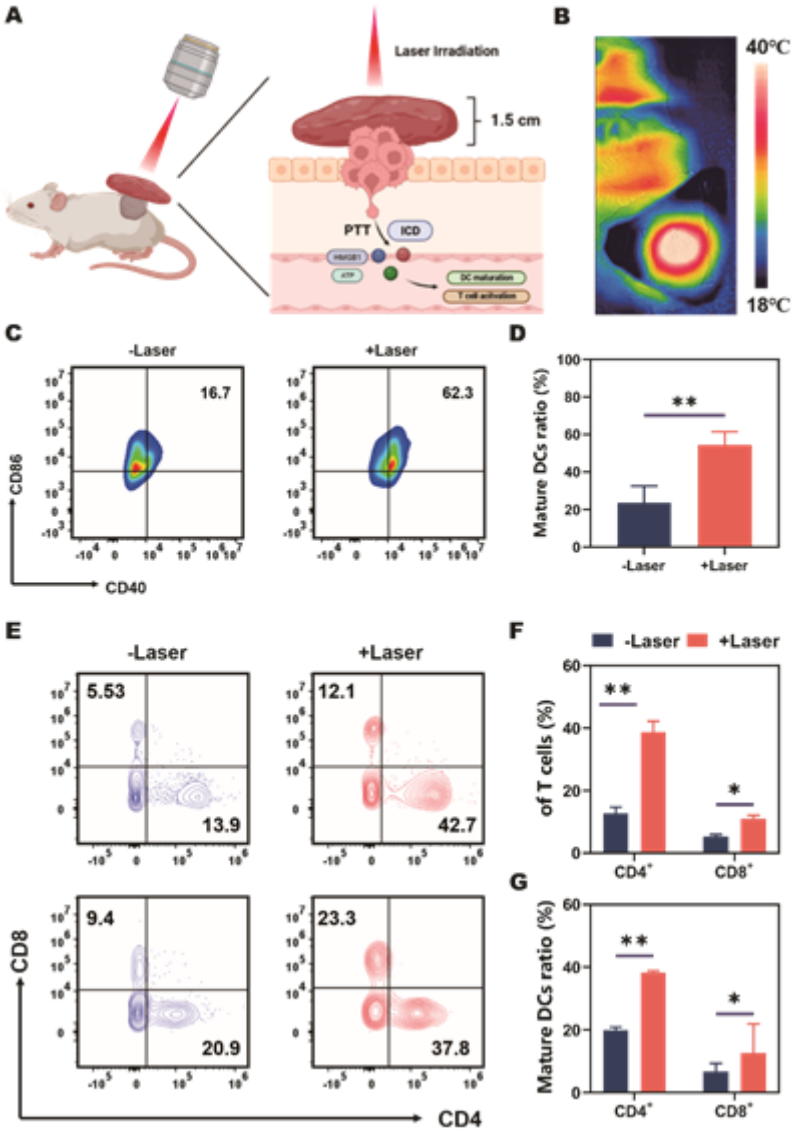

Figure 7. Immunomodulatory effect of SPRIN-micelle in simulated deep-seated tumor model. A) Illustration of experimental setup of deep-seated tumor model. B) Thermal images of CT26 tumor-bearing mice during 940 nm photoirradiation (1 W cm^{-2}) at 24 h post-injection of SPRIN-micelle. C, D) DC maturation measured by flow cytometry after cells in tumor-draining lymph nodes were collected and stained with CD11c, CD40 and CD86 on day 3 (n = 3). E) Representative flow analysis of $CD8^+$ and $CD4^+$ cells gating on $CD3^+$ cells in

the spleen and tumor with different treatments on day **3** (n = 3). The value of $CD8^+$ and $CD4^+$ in spleen and tumor after different treatments (n = 3). Statistical significance was calculated via one-way ANOVA with Tukey's test: *p < 0.05; **p < 0.01; ***p < 0.001; ****p < 0.0001

Conclusion

In summary, we developed a dual polymeric photothermal immunomic nanomicelle for the combined photothermal immunotherapy of cold tumors featuring TiME. This work not only illustrates the effective treatment of primary tumors and the inhibition of tumor metastasis by photothermal immunotherapy, but also reveals the synergistic enhancement of immune response by combination of different immunotherapeutic pathways. In addition, the efficacy of photothermal immunotherapy using laser with different wavelengths were also compared, demonstrating that a NIR-II laser with longer wavelength and higher concentrations induced more pronounced photothermal immunotherapy for solid tumor ablation and anti-tumor immune activation owing to the rational design of this new SP and CMC-switching technology. Taken together, SPRIN-micelles represent a promising biomaterial that enables thermal immunotherapy and metabolic modulation for the treatment of deep-seated tumors.

Statistical Analysis

Data are given as mean ± standard deviation (SD). Flow cytometry results were analyzed with FlowJo v10. The statistical significance of tumor growth and survival rates was calculated via two-way ANOVA with Tukey's test and log-rank test, respectively. For multiple comparisons, one-way analysis of variance (ANOVA) with Tukey's post hoc test was used. The level of significance was defined as *$p < 0.05$, **$p < 0.01$, ***$p < 0.001$, ****$p < 0.0001$. All statistical analyses were performed using GraphPad Prism 8.0 software.

ASSOCIATED CONTENT

Supporting Information

Experimental details, materials, methods, and ^{1}H, ^{13}C-NMR and HR/MS spectra for all compounds.

AUTHOR INFORMATION

Corresponding author

Yumiao Zhang-School of Chemical Engineering and Technology, Key Laboratory of Systems Bioengineering (Ministry of Education), Tianjin University, Tianjin, P. R. China 300350; Orcid https://orcid.org/0000-0002-6166-0470; Email: ymzhang88@tju.edu.cn

Authors

Gengqi Liu-School of Chemical Engineering and Technology, Key Laboratory of Systems Bioengineering (Ministry of Education), Tianjin University, Tianjin, P. R. China 300350

Jiexin Li- School of Chemical Engineering and Technology, Key Laboratory of Systems Bioengineering (Ministry of Education), Tianjin University, Tianjin, P. R. China 300350

Xiaojie Wang- School of Chemical Engineering and Technology, Key Laboratory of Systems Bioengineering (Ministry of Education), Tianjin University, Tianjin, P. R. China 300350

Ren He- School of Chemical Engineering and Technology, Key Laboratory of Systems Bioengineering (Ministry of Education), Tianjin University, Tianjin, P. R. China 300350

Author Contributions

G.L. and Y.Z. conceived the project. G.L. carried out most of the experiments. J.L.and X.W. assisted with the animal experiments. G.L. and Y.Z. performed data analysis and wrote the manuscript.

Notes

The authors declare no competing financial interest.

ACKNOWLEDGEMENTS

This work was supported by National Natural Science Foundation of China (32071384), the National Key Research and Development Program (2021YFC2102300), Start-up Grant at Tianjin University and One-thousand Young Talent Program of China.

Ethical statement

All animal procedures were performed in accordance with the guidelines for Care and Use of Laboratory Animals of Tianjin University, and approved by the Animal Ethics Committee of Tianjin University. The assigned approval number is TJUE-2023-025.

Reference

[1] I. Mellman, G. Coukos, G. Dranoff, Cancer immunotherapy comes of age, Nature, 480 (2011) 480-489.

[2] S.A. Rosenberg, J.C. Yang, N.P. Restifo, Cancer immunotherapy: moving beyond current vaccines, Nature Medicine, 10 (2004) 909-915.

[3] P. Bonaventura, T. Shekarian, V. Alcazer, J. Valladeau-Guilemond, S. Valsesia-Wittmann, S. Amigorena, C. Caux, S. Depil, Cold Tumors: A Therapeutic Challenge for Immunotherapy, Frontiers in Immunology, 10 (2019).

[4] S. Spranger, Mechanisms of tumor escape in the context of the T-cell-inflamed and the non-T-cell-inflamed tumor microenvironment, International Immunology, 28 (2016) 383-391.

[5] Q. Chen, T. Sun, C. Jiang, Recent Advancements in Nanomedicine for 'Cold' Tumor Immunotherapy, Nano-Micro Letters, 13 (2021) 92.

[6] L. Dai, M. Yao, Z. Fu, X. Li, X. Zheng, S. Meng, Z. Yuan, K. Cai, H. Yang, Y. Zhao, Multifunctional metal-organic framework-based nanoreactor for starvation/oxidation improved indoleamine 2,3-dioxygenase-blockade tumor immunotherapy, Nature Communications, 13 (2022) 2688.

[7] M. Wang, M. Chang, C. Li, Q. Chen, Z. Hou, B. Xing, J. Lin, Tumor-Microenvironment-Activated Reactive Oxygen Species Amplifier for Enzymatic Cascade Cancer Starvation/Chemodynamic /Immunotherapy, Advanced Materials, 34 (2022) 2106010.

[8] X. Li, T. Yong, Z. Wei, N. Bie, X. Zhang, G. Zhan, J. Li, J. Qin, J. Yu, B. Zhang, L. Gan, X. Yang, Reversing insufficient photothermal therapy-induced tumor relapse and metastasis by regulating cancer-associated fibroblasts, Nature Communications, 13 (2022) 2794.

[9] Z. Zeng, C. Zhang, J. Li, D. Cui, Y. Jiang, K. Pu, Activatable Polymer Nanoenzymes for Photodynamic Immunometabolic Cancer Therapy, Advanced Materials, 33 (2021) 2007247.

[10] Q. Chen, J. Chen, Z. Yang, J. Xu, L. Xu, C. Liang, X. Han, Z. Liu, Nanoparticle-Enhanced Radiotherapy to Trigger Robust Cancer Immunotherapy, Advanced Materials, 31 (2019) 1802228.

[11] C. Ji, M. Zhao, C. Wang, R. Liu, S. Zhu, X. Dong, C. Su, Z. Gu, Biocompatible Tantalum Nanoparticles as Radiosensitizers for Enhancing Therapy Efficacy in Primary Tumor and Metastatic Sentinel Lymph Nodes, ACS Nano, 16 (2022) 9428-9441.

[12] X. Li, J.F. Lovell, J. Yoon, X. Chen, Clinical development and potential of photothermal and photodynamic therapies for cancer, Nature Reviews Clinical Oncology, 17 (2020) 657-674.

[13] L. Zou, H. Wang, B. He, L. Zeng, T. Tan, H. Cao, X. He, Z. Zhang, S. Guo, Y. Li, Current Approaches of Photothermal Therapy in Treating Cancer Metastasis with Nanotherapeutics, in: Theranostics, 2016, pp. 762-772.

[14] D.V. Krysko, A.D. Garg, A. Kaczmarek, O. Krysko, P. Agostinis, P. Vandenabeele, Immunogenic cell death and DAMPs in cancer therapy, Nature Reviews Cancer, 12 (2012) 860-875.

[15] C. Chen, X. Ni, S. Jia, Y. Liang, X. Wu, D. Kong, D. Ding, Massively Evoking Immunogenic Cell Death by Focused Mitochondrial Oxidative Stress using an AIE Luminogen with a Twisted Molecular Structure, Advanced Materials, 31 (2019) 1904914.

[16] X. Li, H. Sun, H. Li, C. Hu, Y. Luo, X. Shi, A. Pich, Multi-Responsive Biodegradable Cationic Nanogels for Highly Efficient Treatment of Tumors, Advanced Functional Materials, 31 (2021) 2100227.

[17] A. Li, X. Li, X. Yu, W. Li, R. Zhao, X. An, D. Cui, X. Chen, W. Li, Synergistic thermoradiotherapy based on PEGylated Cu3BiS3 ternary semiconductor nanorods with strong absorption in the second near-infrared window, Biomaterials, 112 (2017) 164-175.

[18] P. Huang, J. Lin, W. Li, P. Rong, Z. Wang, S. Wang, X. Wang, X. Sun, M. Aronova, G. Niu, R.D. Leapman, Z. Nie, X. Chen, Biodegradable Gold Nanovesicles with an Ultrastrong Plasmonic Coupling Effect for Photoacoustic Imaging and Photothermal Therapy, Angewandte Chemie International Edition, 52 (2013) 13958-13964.

[19] T. He, C. Jiang, J. He, Y. Zhang, G. He, J. Wu, J. Lin, X. Zhou, P. Huang, Manganese-Dioxide-Coating-Instructed Plasmonic Modulation of Gold Nanorods for Activatable Duplex-Imaging-Guided NIR-II Photothermal-Chemodynamic Therapy, Advanced Materials, 33 (2021) 2008540.

[20] Y. Yang, Y. Chen, P. Pei, Y. Fan, S. Wang, H. Zhang, D. Zhao, B.-Z. Qian, F. Zhang, Fluorescence-amplified nanocrystals in the second near-infrared window for in vivo real-time dynamic multiplexed imaging, Nature Nanotechnology, (2023).

[21] J. Shao, J. Zhang, C. Jiang, J. Lin, P. Huang, Biodegradable titanium nitride MXene quantum dots for cancer phototheranostics in NIR-I/II biowindows, Chemical Engineering Journal, 400 (2020) 126009.

[22] G. Hong, S. Diao, J. Chang, A.L. Antaris, C. Chen, B. Zhang, S. Zhao, D.N. Atochin, P.L. Huang, K.I. Andreasson, C.J. Kuo, H. Dai, Through-skull fluorescence imaging of the brain in a new near-infrared window, Nature Photonics, 8 (2014) 723-730.

[23] K. Welsher, S.P. Sherlock, H. Dai, Deep-tissue anatomical imaging of mice using carbon nanotube fluorophores in the second near-infrared window, Proceedings of the National Academy of Sciences, 108 (2011) 8943-8948.

[24] X. Yao, B. Yang, C. Li, Q. He, W. Yang, Second Near-infrared Light-activatable CO nanogenerator for enhanced cancer Photo-theranostics, Chemical Engineering Journal, 453 (2023) 139888.

[25] K. Shimomura, H. Kai, Y. Nakamura, Y. Hong, S. Mori, K. Miki, K. Ohe, Y. Notsuka, Y. Yamaoka, M. Ishida, D. Kim, H. Furuta, Bis-Metal Complexes of Doubly N-Confused Dioxohexaphyrins as Potential Near-Infrared-II Photoacoustic Dyes, Journal of the American Chemical Society, 142 (2020) 4429-4437.

[26] H. Pan, S. Li, J.-I. Kan, L. Gong, C. Lin, W. Liu, D. Qi, K. Wang, X. Yan, J. Jiang, A cruciform phthalocyanine pentad-based NIR-II photothermal agent for highly efficient tumor ablation, Chemical Science, 10 (2019) 8246-8252.

[27] J.W. Jang, B. Gopal, S.J. Park, S.G. Lee, J.S. Park, Outstanding near-infrared absorption and photothermal conversion properties of phosphorus(V)-phthalocyanines containing diverse axial substituents, Dyes and Pigments, 212 (2023) 111132.

[28] Z. Feng, X. Yu, M. Jiang, L. Zhu, Y. Zhang, W. Yang, W. Xi, G. Li, J. Qian, Excretable IR-820 for in vivo NIR-II fluorescence cerebrovascular imaging and photothermal therapy of subcutaneous tumor, Theranostics, 9 (2019) 5706-5719.

[29] B. Li, L. Lu, M. Zhao, Z. Lei, F. Zhang, An Efficient 1064 nm NIR-II Excitation Fluorescent Molecular Dye for Deep-Tissue High-Resolution Dynamic Bioimaging, Angewandte Chemie International Edition, 57 (2018) 7483-7487.

[30] K. Wen, H. Tan, Q. Peng, H. Chen, H. Ma, L. Wang, A. Peng, Q. Shi, X. Cai, H. Huang, Achieving Efficient NIR-II Type-I Photosensitizers for Photodynamic/Photothermal Therapy upon Regulating Chalcogen Elements, Advanced Materials, 34 (2022) 2108146.

[31] Y. Yang, X. Fan, L. Li, Y. Yang, A. Nuernisha, D. Xue, C. He, J. Qian, Q. Hu, H. Chen, J. Liu, W. Huang, Semiconducting Polymer Nanoparticles as Theranostic System for Near-Infrared-II Fluorescence Imaging and Photothermal Therapy under Safe Laser Fluence, ACS Nano, 14 (2020) 2509-2521.

[32] Y. Jiang, P.K. Upputuri, C. Xie, Z. Zeng, A. Sharma, X. Zhen, J. Li, J. Huang, M. Pramanik, K. Pu, Metabolizable Semiconducting Polymer Nanoparticles for Second Near-Infrared Photoacoustic Imaging, Advanced Materials, 31 (2019) 1808166.

[33] J. Li, X. Yu, Y. Jiang, S. He, Y. Zhang, Y. Luo, K. Pu, Second Near-Infrared Photothermal Semiconducting Polymer Nanoadjuvant for Enhanced Cancer Immunotherapy, Advanced Materials, 33 (2021) 2003458.

[34] Y. Ding, B. Park, J. Ye, X. Wang, G. Liu, X. Yang, Z. Jiang, M. Han, Y. Fan, J. Song, C. Kim, Y. Zhang, Surfactant-Stripped Semiconducting Polymer Micelles for Tumor Theranostics and Deep Tissue Imaging in the NIR-II Window, Small, 18 (2022) 2104132.

[35] D. Moukheiber, U. Chitgupi, K.A. Carter, D. Luo, B. Sun, S. Goel, C.A. Ferreira, J.W. Engle, D. Wang, J. Geng, Y. Zhang, J. Xia, W. Cai, J.F. Lovell, Surfactant-Stripped Pheophytin Micelles for Multimodal Tumor Imaging and Photodynamic Therapy, ACS Applied Bio Materials, 2 (2019) 544-554.

[36] Y. Zhang, H. Hong, B. Sun, K. Carter, Y. Qin, W. Wei, D. Wang, M. Jeon, J. Geng, R.J. Nickles, G. Chen, P.N. Prasad, C. Kim, J. Xia, W. Cai, J.F. Lovell, Surfactant-stripped naphthalocyanines for multimodal tumor theranostics with upconversion guidance cream, Nanoscale, 9 (2017) 3391-3398.

[37] Y. Zhou, D. Wang, Y. Zhang, U. Chitgupi, J. Geng, Y. Wang, Y. Zhang, T.R. Cook, J. Xia, J.F. Lovell, A Phosphorus Phthalocyanine Formulation with Intense Absorbance at 1000 nm for Deep Optical Imaging, Theranostics, 6 (2016) 688-697.

[38] Y. Zhang, M. Jeon, L.J. Rich, H. Hong, J. Geng, Y. Zhang, S. Shi, T.E. Barnhart, P. Alexandridis, J.D. Huizinga, M. Seshadri, W. Cai, C. Kim, J.F. Lovell, Non-invasive multimodal functional imaging of the intestine with frozen micellar naphthalocyanines, Nature Nanotechnology, 9 (2014) 631-638.

[39] Y. Zhang, W. Song, J. Geng, U. Chitgupi, H. Unsal, J. Federizon, J. Rzayev, D.K. Sukumaran, P. Alexandridis, J.F. Lovell, Therapeutic surfactant-stripped frozen micelles, Nature Communications, 7 (2016) 11649.

[40] Y. Zhang, D. Wang, S. Goel, B. Sun, U. Chitgupi, J. Geng, H. Sun, T.E. Barnhart, W. Cai, J. Xia, J.F. Lovell, Surfactant-Stripped Frozen Pheophytin Micelles for Multimodal Gut Imaging, Advanced Materials, 28 (2016) 8524-8530.

[41] C.Y. Wu, K.T. Roybal, E.M. Puchner, J. Onuffer, W.A. Lim, Remote control of therapeutic T cells through a small molecule-gated chimeric receptor, Science, 350 (2015) aab4077.

[42] X. Zang, X. Zhao, H. Hu, M. Qiao, Y. Deng, D. Chen, Nanoparticles for tumor immunotherapy, European Journal of Pharmaceutics and Biopharmaceutics, 115 (2017) 243-256.

[43] R. Mahjub, S. Jatana, S.E. Lee, Z. Qin, G. Pauli, M. Soleimani, S. Madadi, S.-D. Li, Recent advances in applying nanotechnologies for cancer immunotherapy, Journal of Controlled Release, 288 (2018) 239-263.

[44] J. Liu, S. He, Y. Luo, Y. Zhang, X. Du, C. Xu, K. Pu, J. Wang, Tumor-Microenvironment-Activatable Polymer Nano-Immunomodulator for Precision Cancer Photoimmunotherapy, Advanced Materials, 34 (2022) 2106654.

[45] W. Nie, G. Wu, J. Zhang, L.-L. Huang, J. Ding, A. Jiang, Y. Zhang, Y. Liu, J. Li, K. Pu, H.-Y. Xie, Responsive Exosome Nano-bioconjugates for Synergistic Cancer Therapy, Angewandte Chemie International Edition, 59 (2020) 2018-2022.

[46] Y.P. Jia, K. Shi, F. Yang, J.F. Liao, R.X. Han, L.P. Yuan, Y. Hao, M. Pan, Y. Xiao, Z.Y. Qian, X.W. Wei, Multifunctional Nanoparticle Loaded Injectable Thermoresponsive Hydrogel as NIR Controlled Release Platform for Local Photothermal Immunotherapy to Prevent Breast Cancer Postoperative Recurrence and Metastases, Advanced Functional Materials, 30 (2020) 2001059.

[47] S. Fu, L. Chang, S. Liu, T. Gao, X. Sang, Z. Zhang, W. Mu, X. Liu, S. Liang, H. Yang, H. Yang, Q. Ma, Y. Liu, N. Zhang, Temperature sensitive liposome based cancer nanomedicine enables tumour lymph node immune microenvironment remodelling, Nature Communications, 14 (2023) 2248.

[48] F. Zhang, F. Chen, C. Yang, L. Wang, H. Hu, X. Li, X. Zheng, Z. Wang, Z. Chang, T. Li, L. Li, M. Ge, J. Du, W. Sun, W.-f. Dong, D. Shao, Coordination and Redox Dual-Responsive Mesoporous Organosilica Nanoparticles Amplify Immunogenic Cell Death for Cancer Chemoimmunotherapy, Small, 17 (2021) 2100006.

[49] Y. Xiao, T. Zhang, X. Ma, Q.-C. Yang, L.-L. Yang, S.-C. Yang, M. Liang, Z. Xu, Z.-J. Sun, Microenvironment-Responsive Prodrug-Induced Pyroptosis Boosts Cancer Immunotherapy, Advanced Science, 8 (2021) 2101840.

[50] H. Xia, M. Qin, Z. Wang, Y. Wang, B. Chen, F. Wan, M. Tang, X. Pan, Y. Yang, J. Liu, R. Zhao, Q. Zhang, Y. Wang, A pH-/Enzyme-Responsive Nanoparticle Selectively Targets Endosomal Toll-like Receptors to Potentiate Robust Cancer Vaccination, Nano Letters, 22 (2022) 2978-2987.

[51] K. Cheng, Y. Ding, Y. Zhao, S. Ye, X. Zhao, Y. Zhang, T. Ji, H. Wu, B. Wang, G.J. Anderson, L. Ren, G. Nie, Sequentially Responsive Therapeutic Peptide Assembling Nanoparticles for Dual-Targeted Cancer Immunotherapy, Nano Letters, 18 (2018) 3250-3258.

[52] N. Gong, Y. Zhang, X. Teng, Y. Wang, S. Huo, G. Qing, Q. Ni, X. Li, J. Wang, X. Ye, T. Zhang, S. Chen, Y. Wang, J. Yu, P.C. Wang, Y. Gan, J. Zhang, M.J. Mitchell, J. Li, X.-J. Liang, Proton-driven transformable nanovaccine for cancer immunotherapy, Nature Nanotechnology, 15 (2020) 1053-1064.

[53] W. Yang, H. Deng, S. Zhu, J. Lau, R. Tian, S. Wang, Z. Zhou, G. Yu, L. Rao, L. He, Y. Ma, X. Chen, Size-transformable antigen-presenting cell–mimicking nanovesicles potentiate effective cancer immunotherapy, Science Advances, 6 eabd1631.

[54] B. Wang, S. Van Herck, Y. Chen, X. Bai, Z. Zhong, K. Deswarte, B.N. Lambrecht, N.N. Sanders, S. Lienenklaus, H.W. Scheeren, S.A. David, F. Kiessling, T. Lammers, B.G. De Geest, Y. Shi, Potent and Prolonged Innate Immune Activation by Enzyme-Responsive Imidazoquinoline TLR7/8 Agonist Prodrug Vesicles, Journal of the American Chemical Society, 142 (2020) 12133-12139.

[55] C.M. Brackett, B. Kojouharov, J. Veith, K.F. Greene, L.G. Burdelya, S.O. Gollnick, S.I. Abrams, A.V. Gudkov, Toll-like receptor-5 agonist, entolimod, suppresses metastasis and induces immunity by stimulating an NK-dendritic-CD8+ T-cell axis, Proceedings of the National Academy of Sciences, 113 (2016) E874-E883.

[56] J. Li, H. Ren, Q. Qiu, X. Yang, J. Zhang, C. Zhang, B. Sun, J.F. Lovell, Y. Zhang, Manganese Coordination Micelles That Activate Stimulator of Interferon Genes and Capture In Situ Tumor Antigens for Cancer Metalloimmunotherapy, ACS Nano, 16 (2022) 16909-16923.

[57] M.H. den Brok, C. Büll, M. Wassink, A.M. de Graaf, J.A. Wagenaars, M. Minderman, M. Thakur, S. Amigorena, E.O. Rijke, C.C. Schrier, G.J. Adema, Saponin-based adjuvants induce cross-presentation in dendritic cells by intracellular lipid body formation, Nature Communications, 7 (2016) 13324.

[58] L. Chen, H. Qin, R. Zhao, X. Zhao, L. Lin, Y. Chen, Y. Lin, Y. Li, Y. Qin, Y. Li, S. Liu, K. Cheng, H. Chen, J. Shi, G.J. Anderson, Y. Wu, Y. Zhao, G. Nie, Bacterial cytoplasmic membranes synergistically enhance the antitumor activity of autologous cancer vaccines, Science Translational Medicine, 13 (2021) eabc2816.

[59] A.G. Pockley, Heat shock proteins as regulators of the immune response, The Lancet, 362 (2003) 469-476.

[60] J.M. Ramanjulu, G.S. Pesiridis, J. Yang, N. Concha, R. Singhaus, S.-Y. Zhang, J.-L. Tran, P. Moore, S. Lehmann, H.C. Eberl, M. Muelbaier, J.L. Schneck, J. Clemens, M. Adam, J. Mehlmann, J. Romano, A. Morales, J. Kang, L. Leister, T.L. Graybill, A.K. Charnley, G. Ye, N. Nevins, K. Behnia, A.I. Wolf, V. Kasparcova, K. Nurse, L. Wang, A.C. Puhl, Y. Li, M. Klein, C.B. Hopson, J. Guss, M. Bantscheff, G. Bergamini, M.A. Reilly, Y. Lian, K.J. Duffy, J. Adams, K.P. Foley, P.J. Gough, R.W. Marquis, J. Smothers, A. Hoos, J.

Bertin, Design of amidobenzimidazole STING receptor agonists with systemic activity, Nature, 564 (2018) 439-443.

[61] G.J. Weiner, CpG oligodeoxynucleotide-based therapy of lymphoid malignancies, Advanced Drug Delivery Reviews, 61 (2009) 263-267.

[62] M. Liu, X. Wang, L. Wang, X. Ma, Z. Gong, S. Zhang, Y. Li, Targeting the IDO1 pathway in cancer: from bench to bedside, Journal of Hematology & Oncology, 11 (2018) 100.

[63] C. Sheridan, IDO inhibitors move center stage in immuno-oncology, Nature Biotechnology, 33 (2015) 321-322.

[64] T. Komiya, C.H. Huang, Updates in the Clinical Development of Epacadostat and Other Indoleamine 2,3-Dioxygenase 1 Inhibitors (IDO1) for Human Cancers, Frontiers in Oncology, 8 (2018).

[65] M. Jurk, F. Heil, J. Vollmer, C. Schetter, A.M. Krieg, H. Wagner, G. Lipford, S. Bauer, Human TLR7 or TLR8 independently confer responsiveness to the antiviral compound R-848, Nature Immunology, 3 (2002) 499-499.

[66] M.R. Mautino, F.A. Jaipuri, J. Waldo, S. Kumar, J. Adams, C. Van Allen, A. Marcinowicz-Flick, D. Munn, N. Vahanian, C.J. Link, Abstract 491: NLG919, a novel indoleamine-2,3-dioxygenase (IDO)-pathway inhibitor drug candidate for cancer therapy, Cancer Research, 73 (2013) 491-491.

[67] Daniel S. Chen, I. Mellman, Oncology Meets Immunology: The Cancer-Immunity Cycle, Immunity, 39 (2013) 1-10.

[68] A. Gardner, B. Ruffell, Dendritic Cells and Cancer Immunity, Trends in Immunology, 37 (2016) 855-865.

[69] L. Zhai, E. Ladomersky, A. Lenzen, B. Nguyen, R. Patel, K.L. Lauing, M. Wu, D.A. Wainwright, IDO1 in cancer: a Gemini of immune checkpoints, Cellular & Molecular Immunology, 15 (2018) 447-457.

[70] X. Li, M. Wenes, P. Romero, S.C.-C. Huang, S.-M. Fendt, P.-C. Ho, Navigating metabolic pathways to enhance antitumour immunity and immunotherapy, Nature Reviews Clinical Oncology, 16 (2019) 425-441.

SPRIN-micelles induce a cascade of cancer immune responses via deep photothermal therapy. In the presence of elevated intracellular GSH levels, micelles specifically release immune adjuvants (R837) and immune metabolic modulators (IND), thereby promoting dendritic cell maturation and inhibiting IDO-induced hypermetabolism of tryptophan leads to diminished immunosuppression and activation of immune responses.